Tectonophysics, 115 (1985) 61–68
Elsevier Science Publishers B.V., Amsterdam – Printed in The Netherlands

SOURCE GEOMETRY AND MECHANISM OF 1978 TABAS, IRAN, EARTHQUAKE FROM WELL LOCATED AFTERSHOCKS

MANSOUR NIAZI [1] and JAFAR SHOJA-TAHERI [2]

[1] *TERA Corporation, 2150 Shattuck Ave., Berkeley, CA 94704 (U.S.A.)*
[2] *Mashad University, Mashad (Iran)*

(Received September 24, 1984; revised version accepted November 20, 1984)

ABSTRACT

Niazi, M. and Shoja-Taheri, J., 1985. Source geometry and mechanism of the 1978 Tabas, Iran, earthquake from well located aftershocks. *Tectonophysics*, 115: 61–68.

Aftershocks of the September 16, 1978 Tabas earthquake located from close-in observations made during a four-week fielding of temporary stations have been analyzed for the purpose of delineating detailed source geometry of the 1978 earthquake. Spatial distribution of aftershocks and their composite focal mechanism suggest that the geometry of faulting is far from planar. Aftershocks define two prominent alignment. The southern alignment strikes E–W to WNW–ESE, whereas the northern alignment strikes in a N–S to NNW–SSE direction with an abrupt change of nearly 55–60 degrees near 33.4°N latitude. Both field observations of surface faulting pattern and systematic variation of principal directions of stress axes computed from aftershock focal mechanisms are consistent with the upthrusting and imbrication of a wedge shaped crustal block with the wedge angle of about 120 degrees. Both geological and seismological evidence suggest that the deformed zone is truncated at the southern edge by preexisting E–W fault structures. New observations may provide a partial answer to the unexplained farfield asymmetry of the long period Rayleigh wave radiation pattern recently observed for the mainshock across IDA network.

INTRODUCTION

On September 16, 1978, a destructive earthquake with an estimated M_s 7.3–7.7 occurred in east-central Iran, devastating the town of Tabas and outlying villages to distances as far as 80 km. On the basis of damage, destruction and loss of life in the region, this earthquake has been ranked the strongest during this century (Mohajer Ashjai and Nowroozi, 1979). Several studies have so far analyzed gross geologic, seismologic and engineering aspects of this earthquake (Berberian et al., 1979; Hadley et al., 1983; Niazi, 1984). Because the Tabas acceleration time history written in the near-field of a major shallow earthquake with mapped surface faulting has proven to be of great interest to the engineers, we here address in more detail some

0040-1951/85/$03.30

of the inferred complexities of the mainshock source by considering the spatial distribution of aftershocks and their focal mechanism pattern.

FIELD STUDY

Shortly after the occurrence of the Tabas earthquake, a set of portable short-period MEQ-800 seismographs was deployed in the epicentral area by the Geophysics Department of Mashad University. As part of the University's permanent seismographic network, KHI, TGH, MUI and SHD at epicentral distances of about 160, 200, 390 and 380 km, respectively, were the closest stations of the network in operation to the east and north of the mainshock epicenter. The location of additional temporary stations used in this study is shown in Fig. 1. The five temporary stations ran for approximately four weeks after which ZG alone continued operation in a permanent capacity. During the four week field operation of the temporary network several hundred aftershocks were recorded of which approximately 180 were located. A listing of the aftershock activity through the end of 1978 is being published in BSSMU (1984). Here we focus on those aftershocks which occurred in the time interval between September 22 and October 22, 1978, and for which the readings of temporary stations were available.

AFTERSHOCK ZONE

The hypocentral coordinates of the mainshock given by NEIS are 33.386°N, 57.434°E with a normal depth. Based on the regional phases alone, the location of mainshock, with a constrained focal depth of 5 km, is several kilometers south of the NEIS epicenter at 33.342°N and 57.400°E well within the accuracy of teleseismic locations in this region. The aftershock zone covers a triangular area of which the obtuse angle opens in the northeast directions and is bounded by approximately N and ESE directions. These directions are parallel to the main trends of the complex system of faulting associated with the earthquake (Berberian, 1982). The aftershock foci for the most part are confined to the highly deformed wedge bounded by and upthrusted along two intersecting planar segments one of which strikes nearly in the N–S direction and dips to the east with the second one striking ESE and dipping to the NNE. This pattern of faulting is also reflected in the abrupt reorientation of aftershock alignment at approximately 33.4°N latitude. South of this latitude the observed alignment is WNW–ESE, whereas to the north the alignment shifts to a more northerly direction. Clearly emerging from the scatter caused partially by location uncertainties in Fig. 1, this abrupt change of alignment can also be seen in fig. 6 of Berberian (1982) in which the best located aftershocks he studied are plotted. A plot of 48 best located events screened under more restricted criteria (Fig. 2) further enhances the suggested realignment.

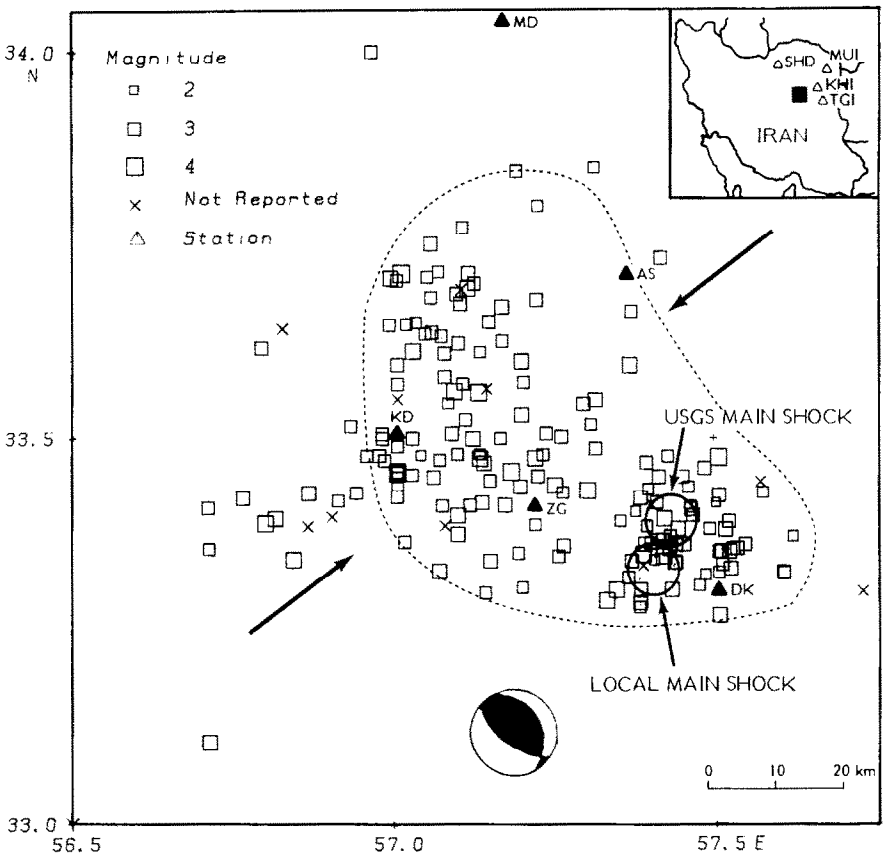

Fig. 1. Aftershock area of the 1978 Tabas earthquake relative to the locations of the mainshock as determined from teleseismic (U.S.G.S.) and regional (Mashad University) data. The dashed line shows limit of faulting and ground disturbance. The location of permanent stations in the inset and temporary stations in the figure are shown by solid triangles. The arrows show the direction of the regional tectonic compression as inferred from the fault plane solution of the main shock, also reproduced in the figure.

The hypocentral location of Figs. 1 and 2 were computed by the application of Hypo-71 program (Lee and Lahr, 1975). The crustal structure used for this purpose is derived from several years of regional data and consists of a 41.3 km thick double layered crust overlying a half-space with the following parameters:

Layer thickness (km)	Compressional velocity (km/sec)	Shear wave velocity (km/sec)
1.3	3.50	2.00
40.0	5.64	3.22
	7.98	4.56

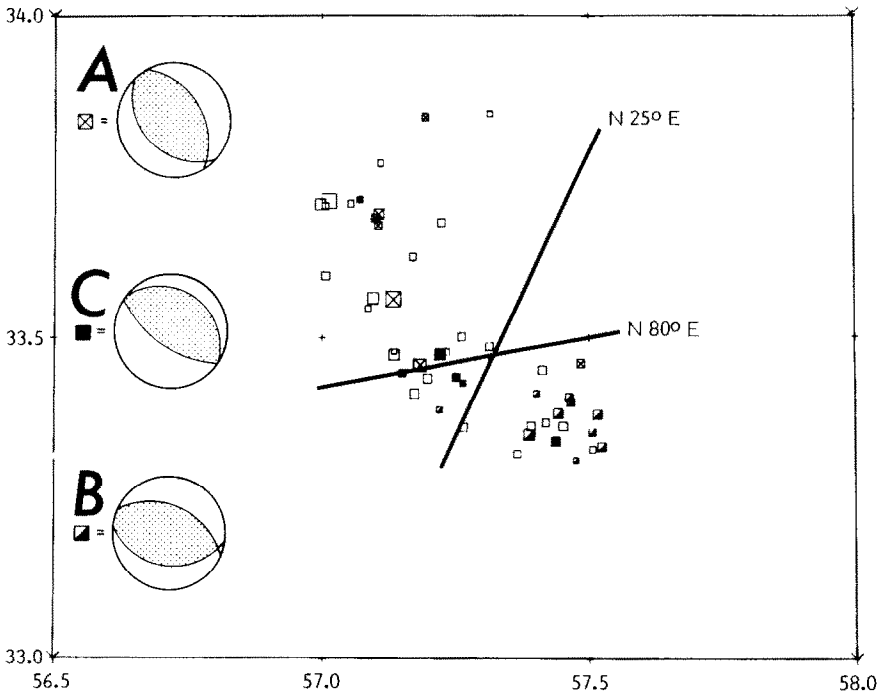

Fig. 2. The epicentral distribution of the 48 well-located (A-events) aftershocks. The two heavy lines are the surface trace of the projection planes of Figs. 3 and 4. The symbols for three subgroups of aftershocks are keyed to their respective composite fault plane solutions.

The selection criteria for screening the events of Fig. 2 are a minimum of six phases, including at least one S reading, standard deviation of solutions of less than 0.4 sec and azimuthal coverage gap of less than 200 degrees.

Two projections of the well located foci of Fig. 2 onto the vertical planes parallel to the N80°E and N25°E directions are shown in Figs. 3 and 4, respectively. The focal depths vary between 0.0 and 18.5 km with a greater concentration between 10 and 15 km. Surface traces of the planes of projection are shown in Fig. 2. The N80°E profile suggests an overall deepening of foci to the east-northeast. The trend is better identified by the larger aftershocks lying to the western edge of the deformed zone. Vertical exaggeration for the N80°E profile is approximately three. The eastward dip of the base of the aftershock zone as shown by the dashed line is nearly 30°.

Except for the three small events to the northern edge of the zone which define a shallow dipping alignment (20° dip) to the northeast, the N25°E profile of Fig. 4 by and large indicates a well defined near vertical alignment with a denser clustering near the southern edge of the zone. With a vertical exaggeration of 5, some of the observed deviations from vertical alignment of denser clusters on the N25°E cross-section may be locally significant; however, the location accuracies may not

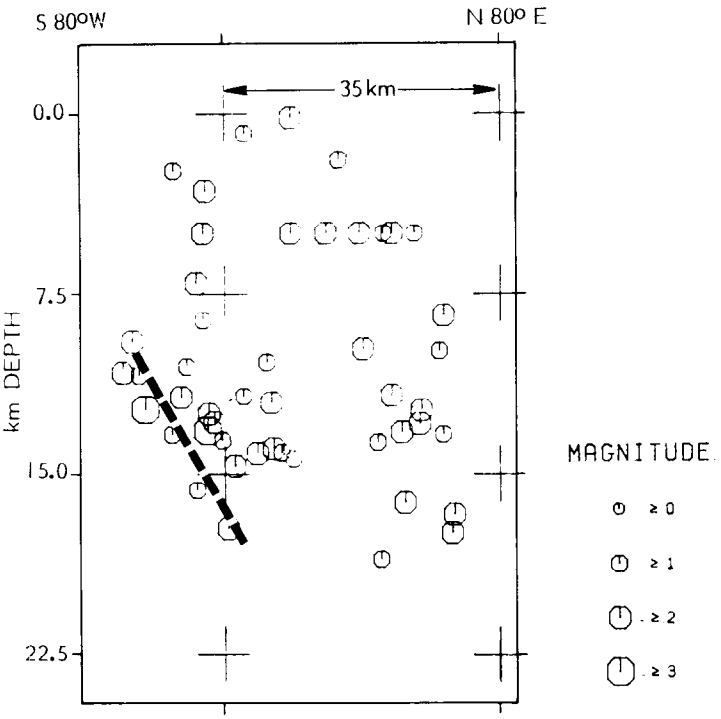

Fig. 3. Projection of the selected hypocenters of Fig. 2 onto the N80°E–S80°W vertical plane. Vertical exaggeration is approximately 3. The slope of the dashed line at the base and to the west of the section is 30°, the same as found in the first motion study of the main shock (Berberian et al., 1979).

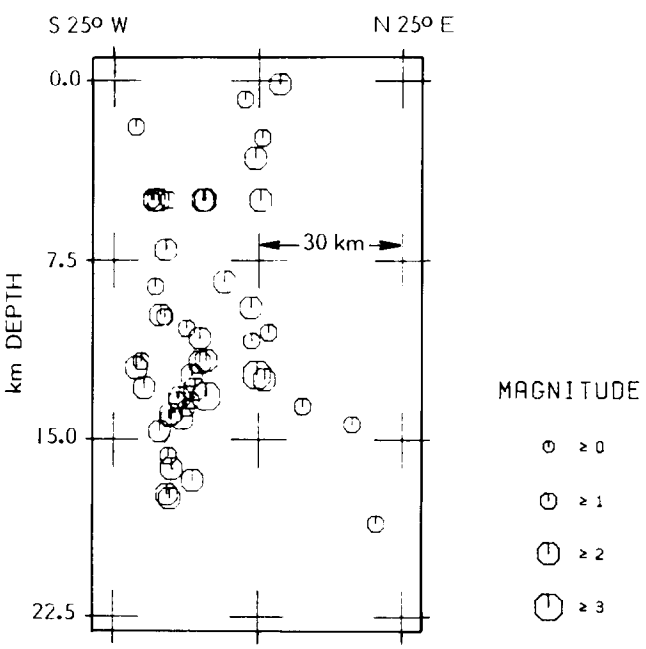

Fig. 4. Vertical projection of selected hypocenters on the N25°E–S25°W profile. Vertical exaggeration is approximately 5.

warrant further resolution of these deviations. Our preferred interpretation of the observed vertical alignment on this profile favors existence of a nearly E–W trending structural boundary near the southern edge of the Tabas plain at about 33.3°N latitude at which deformation is abruptly terminated. No surface expression of such a boundary emerges from the thick sedimentary overburden. However, further south near 33°N latitude, along an east–west trending fault system called Golgolab Fault the recent sedimentary cover of the basin contacts a series of Mesozoic horst (NIOC, 1977) consisting of Jurassic shale and sandstone and cyclically bedded carbonaceous shales of Triassic age (Nayband Formation). Similar controlling transverse structures have been observed for other major earthquakes of this region (Dewey and Grantz, 1973; Haghipour and Amidi, 1980). Also, Mohajer-Ashjai and Nowroozi (1979) have mapped a number of E–W trending secondary fractures which may be considered as surface response to the deep fracturings predicted by the southern alignment.

FOCAL MECHANISM PATTERN

The mainshock's focal mechanism from the P-wave first motion data (Berberian et al., 1979) and Rayleigh wave inversion (Niazi and Kanamori, 1981) best agree with a nearly pure thrust with a NW–SE strike direction. However, the unresolved radiation asymmetry of long period Rayleigh waves observed in the latter study was suspected to require either unexplained regional propagation anomalies (Lay and Kanamori, 1984) or significant complexity of the source (Niazi and Niazi, 1984). To resolve this ambiguity we have examined the focal mechanism pattern of the well located aftershocks by construction of three composite fault plane solutions for (a) the events north of 33.4° latitude, (b) for the events south of this latitude and (c) for all 48 events of Fig. 2.

In construction of composite focal mechanism solutions we have applied the statistical approach (Brillinger et al., 1980; Udias et al., 1982). Setting a lower acceptable consistency ratio of 0.75, and starting with the mainshock solution, the method was applied to the three subgroups of events, independently. As a result 23 of the aftershocks grouped into three solutions, each expressing somewhat different fault plane parameters. The upper hemisphere stereographic projections of the three solutions are also shown in Fig. 2. All three solutions are practically pure thrust mechanism. However, the orientation of stress axes and similarly the strike of fault planes show a systematic counterclockwise rotation as the locations move southward. Seven aftershocks comprising group A are from the subset of the events all located north of 33.4°N latitude. They best agree with a NNW–SSE striking thrust mechanism parallel to their epicentral alignment. All ten aftershocks of group B lie to the south of this latitude and are consistent with a more easterly strike. The six aftershocks of group C belong to the complete set and are dispersed over the whole aftershock zone and the resulting solution is inbetween solutions A and B. The counterclockwise rotation of strike southward as seen in the inset of Fig. 2 is

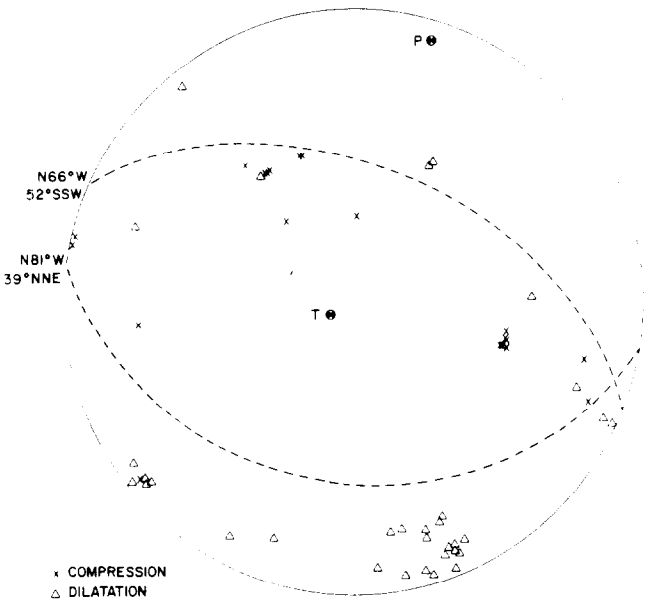

Fig. 5. The projection of first motion polarities of subgroup B on the upper hemisphere.

predicted by the observed reorientation of the aftershock alignment as discussed in the previous section, both of which suggest segmentation of rupture into nonplanar configuration. Figure 5 shows the distribution of first motion data for the ten aftershocks of subgroup B located near the southern boundary. The resulting complexity in the source geometry has been suspected to contribute to the observed asymmetry of the long-period Rayleigh wave radiation (Niazi and Kanamori, 1981).

DISCUSSION

Various lines of evidence, including the alignment of the aftershock pattern, rotation of the composite fault plane solutions, and pattern of surface faulting suggest that the source geometry of the 1978 Tabas earthquake is complex. At minimum two preferred orientation in the NNW–SSE and WNW–ESE are identified which define and control a triangular wedge shape zone of intense deformation and imbrication associated with this earthquake. The apparent segmentation of the fault resulting from the reorientation of the strike by as much as 60° and leading to an arcuate surface fault trace, provides an alternative mechanism for producing the abnormal asymmetry of the observed long-period Rayleigh wave radiation pattern (Niazi and Kanamori, 1981).

ACKNOWLEDGEMENTS

Dr. M. Berberian read the manuscript and provided helpful comments. The logistic support of the Mashad University for the field work is acknowledged. Comments by two anonymous reviewers helped clarify several points.

REFERENCES

Berberian, M., 1982. Aftershock tectonics of the 1978 Tabas-e Golshan (Iran) earthquake sequence: a documented active "thin- and thick-skinned" tectonic case. Geophys. J., 68: 499–530.

Berberian, M., Asudeh, I., Bilham, R.G., Scholtz, C.H. and Soufleris, C., 1979. Mechanism of the main shock and the aftershock study of the Tabas-e-Golshan (Iran) earthquake of September 16, 1978: a preliminary report. Bull. Seismol. Soc. Am., 69: 1851–1859.

Brillinger, D.R., Udias, A. and Bolt, B.A., 1980. A probability model for regional focal mechanism solutions. Bull. Seismol. Soc. Am., 70: 149–170.

BSSMU, 1984. Bulletin of Seismographic Stations of Mashad University, Earthquake Epicenters Listing for July 1–December 31, 1978.

Dewey, J.W. and Grantz, A., 1973. The Ghir earthquake of April 10, 1972 in the Zagros mountains of southern Iran: seismotectonic aspects and some results of a field reconnaissance. Bull. Seismol. Soc. Am., 63: 2071–2090.

Hadley, D.M., Hawkins, H.G. and Benuska, K.L., 1983. Strong ground motion record of the 16 September 1978, Tabas, Iran earthquake. Bull. Seismol. Soc. Am., 73: 315–320.

Haghipour, A. and Amidi, M., 1980. The November 14 to December 25, 1979 Ghaenat earthquakes of northeast Iran and their tectonic implications, Bull. Seismol. Soc. Am., 70: 1751–1757.

Lay, T. and Kanamori, H., 1984. Geometric effects of global lateral heterogeneity on long period surface wave propagation EOS, Trans., Am. Geophys. Union, 65: 244 (abstr.).

Lee, W.H.K. and Lahr, J.C., 1975. Hypo-71: a computer program for determining hypocenter, magnitude first motion pattern of local earthquakes. U.S. Geol. Surv., Open-File Rep. 75-311.

Mohajer-Ashjai, A. and Nowroozi, A.A., 1979. The Tabas earthquake of September 16, 1978 in east-central Iran. Geophys. Res. Lett., 6: 689–692.

Niazi, M., 1984. Estimation of Rupture velocity and nearfield Q from the Tabas accelerogram of the September 16, 1978, Iran earthquake. Proc. 8th World Conf. Earthquake Eng., San Francisco, Vol. 11, pp. 377–383.

Niazi, M. and Kanamori, H., 1981. Source parameters of 1978 Tabas and 1979 Qainat earthquakes from long-period surface waves. Bull. Seismol. Soc. Am., 71: 1201–1213.

Niazi, M. and Niazi, K.F., 1984. Effect of complex source geometry on the surface wave radiation pattern. submitted.

NIOC, 1977. Geological Map of Iran, 1:1000,000 by National Iranian Oil Company.

Udias, A., Buforn, E., Brillinger, D. and Bolt, B.A., 1982. Joint statistical determination of fault-plane parameters. Phys. Earth. Planet. Inter., 30: 178–184.